Surface Water Microwave Product Series Version 3: A Near-Real Time and 25-Year Historical Global Inundated Area Fraction Time Series From Active and Passive Microwave Remote Sensing

Katherine Jensen and Kyle McDonald, *Senior Member, IEEE*

***Abstract*— This letter summarizes substantial modifications made to the Surface Water Microwave Product Series (SWAMPS), a coarse-resolution (∼25 km) global inundated area fraction data record derived from active and passive microwave remote sensing. SWAMPS is the most temporally dense, long-term record of global surface water dynamics publicly available today. This update improves upon the original release by: 1) incorporating a customized, consistent resampling and assembly of the Special Sensor Microwave Imager and Special Sensor Microwave Imager Sounder brightness temperature record; 2) eliminating signal contamination from ocean waters along coastlines; 3) inclusion of permanent surface waters as a component of the data record; and 4) reducing anomalous inundation retrievals over arid and semiarid regions. This update provides for the enhanced scientific utility of the full 25+ years of data records. Remaining uncertainties in the surface water fraction retrievals are principally in areas with bare, sandy surface cover and in areas with dense vegetation cover that diminishes radiometric sensitivity to surface water. This data record and associated documentation are freely available through the Alaska Satellite Facility, Fairbanks, AK, USA.**

***Index Terms*— Inundation, microwave remote sensing, surface water, wetlands.**

I. Introduction

THE extent and dynamics of land surface water tremendously vary across the globe. Accurate and consistent spatial representation of terrestrial inundation is of critical importance for human life and the environment, with essential implications ranging from flood risk and agricultural management to the conservation of biodiversity and other freshwater ecosystem services. The characterization of inundated area dynamics is valuable for wetland studies and for assessing the role of wetlands as major natural sources of atmospheric methane [1], [2].

Available global inventories of the abundance and distribution of dynamic surface waters remain limited [3]. Satellite remote sensing is the only practical approach that can provide continuous monitoring of spatial and temporal land surface dynamics at a global scale. With the recent rise of cloud computing, extensive analysis of multidecadal records of optical satellite imagery (e.g., Landsat) has produced flood recurrence maps at an unprecedented scale (see [4], [5]). However, high-flood seasons and subcanopy inundation are often poorly delineated by optical sensors because of limitations imposed by persistent cloud cover and vegetation cover. Microwave sensors, on the other hand, are not significantly affected by clouds or changing solar illumination and are able to observe surface processes below moderate vegetation cover. High spatial resolution (<100 m) synthetic aperture radar (SAR) provides detailed observations sensitive to flooded land surface but generally provides limited temporal coverage. Sentinel-1 SAR currently provides repeat coverage every 6–12 days, but freely distributed SAR observations at global scales were drastically more infrequent prior to 2014. Coarse-resolution microwave data sets continue to provide utility to the earth system science community today, offering a consistent, retrospective record (30+ years) and temporally rich observations.

The Surface Water Microwave Product Series (SWAMPS) was developed under the NASA Making Earth System Data Records for Use in Research Environments Program and published in 2015 as a global, 20-year record of estimated inundated area fraction (f_w) [6]. SWAMPS was derived from a combination of passive microwave brightness temperature and active microwave radar backscatter using an unmixing algorithm and *a priori* knowledge of land cover. Endmembers representing inundated and noninundated land surfaces are used to derive f_w at 25-km grid cell scale. The inundation dynamics captured by this data set has been utilized in several studies at regional to global scale, with applications ranging from methane emission simulations to assessments of vector-borne disease risk (see [7]–[9]).

We present the release of SWAMPS version 3 (SWAMPSv3), a substantial update to the original SWAMPS release (SWAMPSv2) that includes both a near-real-time (NRT) product and an extended, improved historical record of f_w spanning the past 25+ years (1992–2018). In this letter, we detail the changes in the SWAMPS algorithm and discuss the associated enhancements and remaining uncertainties with this new release.

II. Algorithm Modifications

The same general approach presented by Schroeder *et al.* [6] is employed in the assembly of SWAMPSv3: active microwave backscatter (σ^0) and passive microwave polarization difference index (MPDI) derived from

Manuscript received December 6, 2018; revised January 23, 2019; accepted February 8, 2019. Date of publication March 7, 2019; date of current version August 27, 2019. This work was supported in part by the NASA Making Earth System Data Records for Use in Research Environments Program under Cooperative Agreement NNX11AQ39G and Cooperative Agreement NNX11AP26A, and in part by the NASA Earth and Space Science Fellowship Program under Grant 80NSSC17K038. *(Corresponding author: Katherine Jensen.)*

The authors are with the Department of Earth and Atmospheric Science, NOAA CREST, The City College of New York, New York, NY 10031 USA, with the CUNY CREST Institute, The City College of New York, New York, NY 10031 USA, and also with the Earth and Environmental Sciences Program, The Graduate Center, City University of New York, New York, NY 10016 USA (e-mail: kjensen@ccny.cuny.edu; kmcdonald2@ccny.cuny.edu).

Digital Object Identifier 10.1109/LGRS.2019.2898779

1545-598X © 2019 IEEE. Translations and content mining are permitted for academic research only. Personal use is also permitted, but republication/redistribution requires IEEE permission. See http://www.ieee.org/publications_standards/publications/rights/index.html for more information.

TABLE I
SATELLITE/MODEL SOURCES FOR SWAMPSv3 INPUT DATA SEGMENTS

Input	Segment I. 1992-1999	Segment II. 2000-2008	Segment III. 2009-2018
T_b	SSM/I [a]	SSM/I [a]	SSMIS [a]
σ^0	ERS [b]	QuikSCAT [c]	ASCAT [d]
NDVI	AVHRR [e]	MODIS [f]	MODIS [f]
Snow Cover	SSM/I [g]	MODIS [h]	MODIS [h]
Reanalysis	MERRA-2 [i]	MERRA-2 [i]	MERRA-2 [i]

[a] NOAA Climate Data Record (CDR) of Special Sensor Microwave Imager (SSM/I) and Special Sensor Microwave Imager Sounder (SSMIS) Microwave Brightness Temperatures CSU Version 1 [11]; [b] European Remote Sensing Satellites (ERS-1, ERS-2) Level 1 Product [12]; [c] NASA SeaWinds-on-QuikSCAT Level 1B Sigma0 Product [13]; [d] Advanced Scatterometer (ASCAT) Level 1B Product [14]; [e] Global Inventory Monitoring and Modeling System (GIMMS) NDVI3g.v1 from the Advanced Very High Resolution Radiometer (AVHRR) [15]; [f] MODIS/Terra Vegetation Indices 16-Day L3 Global 0.05 Deg CMG, Version 6 (MOD13C1) [16]; [g] Global Monthly EASE-Grid Snow Water Equivalent Climatology from SSM/I [17]; [h] MODIS/Terra Snow Cover 8-Day L3 Global 0.05 Deg CMG, Version 6 (MOD10C2) [18]; [i] Modern-Era Retrospective analysis for Research and Applications Version 2 (MERRA-2) [10]

brightness temperature (T_b) are the primary inputs to a land cover-supported, atmospherically corrected dynamic mixture model. However, the model now incorporates revised input data and more dynamic land cover information. Ancillary data sources have been updated for improved masking of snow cover and arid land cover. The changes made in the generation of this version are detailed in this section.

A. Input Data Sources

Spanning over 25+ years, the SWAMPS f_w record utilizes a variety of satellite remote sensing data sets that are segmented in three consecutive time series of data source combinations, as summarized in Table I. For the assembly of SWAMPSv3, all microwave observations (passive and active) were obtained at the swath level and processed consistently (details in Section II-B). The hourly atmospheric variables (including total precipitable liquid water, total precipitable water vapor, and wind speed at 2 m height) used in the mixture model for atmospheric correction now draw entirely from the NASA Modern-Era Retrospective analysis for Research and Applications Version 2 (MERRA-2) reanalysis product [10]. Additional ancillary snow cover and normalized difference vegetation index (NDVI) products are used in SWAMPSv3 to mask snow-covered surfaces and to delineate seasonal vegetation dynamics.

B. Processing of Microwave Data

The SWAMPS data record was originally derived in part from daily gridded DMSP Special Sensor Microwave Imager–Special Sensor Microwave Imager Sounder (SSM/I–SSMIS) Pathfinder brightness temperature observations provided by the National Snow and Ice Data Center (NSIDC) [19]. A major processing change in 2008 related to grid interpolation yielded a noticeable difference in the brightness temperature fields of these data. Although in many areas, this difference was within ± 2 K, regions with steep brightness temperature gradients observed discrepancies upward of 20 K. Problematic regions included coastal areas, edges of swaths where the overlap between swaths occurs (typically poleward of 60° latitude), and mountainous regions. Because of this gridding inconsistency, the SWAMPSv2 time series was effectively divided into two distinct parts, hampering long-term analyses. To produce a more consistent, long-term inundation record, swath-level intercalibrated SSM/I (F11 and F13) and SSMIS (F17 and F18) T_b observations were acquired and posted to the 25-km EASE-grid uniformly across the time series using the inverse distance squared (IDS) method. In addition, swath-level radar σ^0 observations were normalized for incidence angle (following an approach introduced by Long and Hardin [20]) and posted to the same 25-km EASE-grid via IDS.

The SWAMPS data record is intended to provide estimates of terrestrial surface water dynamics, including those from wetlands, rivers, small lakes, reservoirs, rice paddies, and episodically inundated areas. In the earlier versions of SWAMPS (< v3), grid cells along coastlines were heavily influenced by ocean water that likely eclipsed the signal from terrestrial inundated surfaces. During the assembly of both T_b and σ^0 for SWAMPSv3, contributions from ocean waters in coastal regions were filtered out using a Landsat-based 90-m mask of permanent ocean waters defined by the G3WBM Global Water Body Map data set [4] and large water bodies such as the Great Lakes and the Caspian and Black Seas.

C. Defining Arid and Semiarid Land Covers

The SWAMPS algorithm estimates erroneously high water fraction over some arid and semiarid regions, including sandy deserts, arid zones, salt pans, and ephemeral water bodies. SWAMPS relies on a static land cover map derived from MODIS [21] and assumes consistent emissivity and backscatter properties over each general International Geosphere-Biosphere Programme (IGBP) land cover class. The anomalous f_w retrievals observed over arid and semiarid regions are associated with the large surface emissivity and backscatter gradients found within the general "Barren or Sparsely Vegetated" (BSV) land cover class across the globe. The variability of microwave measurements observed in this class arise from two primary complicating factors: 1) the emissivity of bare ground is highly influenced by the soil's dominant mineral composition [22] and 2) multitemporal variation in semiarid regions with pronounced seasonal changes in vegetation cover, e.g., Africa's Sahel.

In SWAMPSv3, the general BSV class was partitioned into subsets of bare surface types with similar emissivity and backscatter character. A k-means clustering analysis of the 33 unique surface types identified by the Harmonized World Soil Database (HWSD) [23] was performed based on a climatology of monthly means of gridded 19-GHz MPDI and C-band σ^0 for representative 25 km × 25 km grid cells (>95% BSV, where >85% is represented by a single soil type). Six clusters were selected to segment the general BSV class.

Time series of NDVI was used as a dynamic measure of vegetation cover to delineate arid (permanently nonvegetated) and semiarid (seasonally vegetated) areas. Three statistics were calculated and averaged for both the AVHRR-based record (1992–2000) and MODIS-based record (2000–2018) globally at the original product spatial resolution: 1) annual maximum ($\mathrm{NDVI_{ymax}}$); 2) annual minimum ($\mathrm{NDVI_{ymin}}$); and 3) annual standard deviation ($\mathrm{NDVI_{ystd}}$). Arid and semiarid regions were identified using a definition first developed by Gamo *et al.* [24], and areas labeled as urban, water, or ice by the native 1-km MODIS land cover product (MODIS-IGBP) were excluded. Arid regions were defined as pixels with $\mathrm{NDVI_{ymax}}$ less than 0.15 and $\mathrm{NDVI_{ystd}}$ less than 0.03. Semiarid regions were defined as regions with $\mathrm{NDVI_{ymin}}$ less

than 0.15 and $NDVI_{ystd}$ less than 0.4. The same thresholds were used for both AVHRR- and MODIS-based records.

The fractional land cover map employed by the SWAMPS algorithm was recalculated at each time period (t) an NDVI composite was available (bimonthly for AVHRR and 16 days for MODIS) using subgrid cell, static land cover from MODIS-IGBP, and dynamic vegetation conditions from $NDVI_t$. The general BSV class was eliminated and replaced with six different bare ground classes ("Bare Ground 1–6") and a vegetation class named "Sparse Vegetation." All pixels labeled as BSV by MODIS-IGBP were reclassified to the appropriate bare ground class corresponding to its HWSD soil type. For all pixels identified as semiarid, an additional decision was executed: 1) semiarid BSV pixels with $NDVI_t$ greater than 0.15 were reassigned as "Sparse Vegetation" and 2) semiarid pixels not classified by MODIS-IGBP as BSV but with $NDVI_t$ less than 0.15 were reassigned to their appropriate bare ground class.

The land cover-specific regression models used for approximating seasonal biomass dynamics at each segment (Table I) were redeveloped for each land cover class based on these modified, dynamic land cover maps.

D. Flags

Prior versions of SWAMPS screened for snow cover using a classification and conservative 28-day running average of estimated snow water equivalent (SWE) based on daily T_b observations. This generally overestimated snow cover extent and tends to be overly restrictive, eliminating potentially useful observations after snowpack melt. In this update, we opted to rely on ancillary snow cover products in screening for snow cover. Segment I (Table I) relies on the monthly SWE estimates based on SSM/I [17], similar to what was used in the original version of SWAMPS due to the scarcity of data. However, segments II and III depend on the higher resolution, eight-day MODIS fractional snow cover product [18]. If more than 50% of the MODIS pixels within a 25 km × 25 km grid cell observe a snow fraction greater than 25%, then that grid cell is flagged as snow. Any gaps in the snow cover product are filled with a climatological value derived over the MODIS record, 2000–2017.

Any 25 km × 25 km grid cell that is observed to be greater than 99% arid as defined in Section II-C is flagged as arid. The rationale is that inundation is highly unlikely in these regions and the signal-to-noise ratio is low.

E. Water Fraction Definition

Prior versions of SWAMPS reported the estimated dynamics of nonpermanent surface water area, excluding water bodies and permanently inundated areas. In an effort to facilitate the use of this data set with complementary products, SWAMPSv3 includes all terrestrial water fractions within the f_w retrieval. An ancillary data layer now includes the fractions of permanent water and permanently inundated areas so that they can be accounted for separately, if needed.

III. Results and Discussion

A. Consistency in Brightness Temperature Records

Reprocessing of the swath-level SSM/I and SSMIS T_b record produced a temporally consistent time series. Fig. 1 illustrates globally averaged monthly composites of the 19-GHz MPDI over land comparing the previously used T_b record from NSIDC (NSIDC-Pathfinder) and the newly processed version (Reprocessed NOAA CDR). Comparison of the global average MPDI records from before the change in NSIDC-Pathfinder processing (1992–2008) to

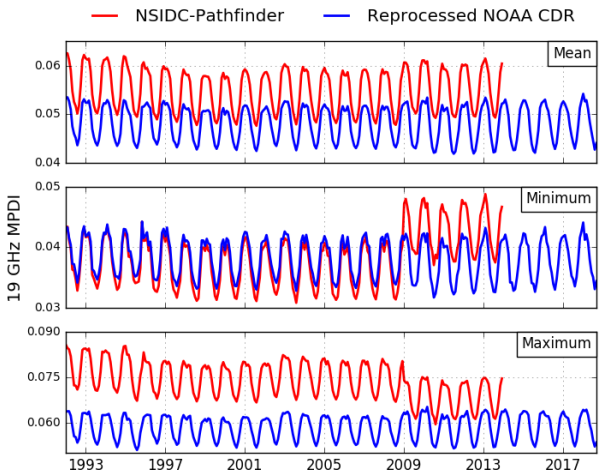

Fig. 1. Globally averaged terrestrial 19-GHz MPDI time series of monthly (Top) means, (Center) minimums, and (Bottom) maximums comparing the previously used NSIDC-Pathfinder record (red) and the reprocessed NOAA CDR record (blue). Spatial averages are screened for snow.

TABLE II
COMPARISON OF MEAN 19-GHz MPDI MONTHLY MEANS, MINIMUMS (MIN), AND MAXIMUMS (MAX) AT T1 (1992–2008) AND T2 (2009–2013)

	NSIDC-Pathfinder			Reprocessed		
	T1	T2	%	T1	T2	%
Mean	0.055	0.056	+1.39%	0.048	0.048	-0.50%
Min	0.037	0.043	+15.9%	0.038	0.038	-2.02%
Max	0.076	0.069	-9.38%	0.058	0.059	+0.43%

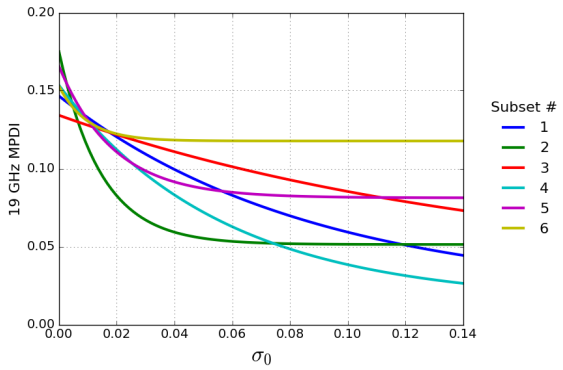

Fig. 2. Relationships between C-band backscatter and 19-GHz MPDI observed by each bare ground subset, derived from monthly means observed during 2009–2017. Corresponding bare surface types that comprise each subset are described in Table III.

after (2009–2013) shows that notable deviations in monthly composite statistics, particularly in the monthly minimums and maximums, have been significantly reduced by the reprocessed record (Table II). Since observations over coastal waters are now filtered, overall terrestrial MPDI values are reduced across the updated record. Investigation of the intercalibration between the SSM/I and SSMIS sensor data sets would support a better understanding of the errors associated with changes in the sensor.

B. Bare Ground Land Cover Subsets

Six clusters of 33 unique HWSD bare surface types were found to best segment the general BSV class, excluding areas classified by HWSD as water, ice, or urban. Fig. 2 depicts the fit relationships between monthly 19-GHz MPDI (SSMIS F17 and F18) and C-band σ^0 (ASCAT), observed from

TABLE III
BARE GROUND CLASS SUBSETS

Subset Number	HWSD Soil/Surface Types	RMSE
1	leptosols, regosols, rock outcrop	0.0169
2	anthrosols, ferralsols, gleysols, kastanozems, lixisols, planosols	0.0146
3	calcisols, solonchaks, salt flats	0.0212
4	acrisols, alisols, chernozems, cambisols, luvisols, phaeozems, plinthosols, podzols, solonetz, vertisols	0.0168
5	andosols, fluvisols, greyzems, gypsisols, histosols, podzoluvisols	0.0190
6	arenosols, sand dunes	0.0323

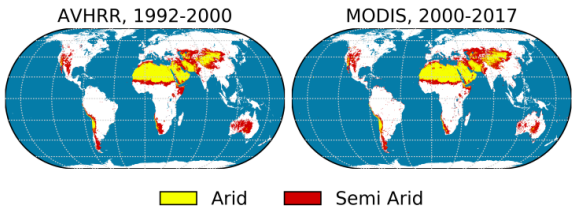

Fig. 3. Delineation of arid and semiarid zones from (Left) AVHRR-based NDVI observations during 1992–2000 and (Right) MODIS-based NDVI observations during 2000–2017.

TABLE IV
DISTRIBUTION OF IGBP LAND COVER CLASSES OBSERVED IN ARID AND SEMIARID REGIONS

	IGBP Land Cover Distribution	AVHRR 1992-2000	MODIS 2000-2017
Arid	Barren / Sparse Vegetation	95.4%	94.7%
	Open Shrubland	2.40%	2.95%
	Grassland	1.99%	2.24%
	Other	< 1%	< 1%
Semi-Arid	Open Shrubland	40.1%	40.7%
	Grassland	30.2%	32.9%
	Barren / Sparse Vegetation	22.3%	24.1%
	Cropland / Natural Vegetation Mosaic	4.69%	1.95%
	Other	< 1%	< 1%

2009 to 2017, for each bare ground class subset. Table III summarizes the HWSD constituents of each subset and the corresponding root-mean-square error (RMSE) observed in each fit displayed in Fig. 2. Bare ground subset 6, which represents sandy surfaces, observed notably greater RMSE than the other subsets.

C. Distinction of Arid and Semiarid Regions

Analysis of NDVI derived from both AVHRR and MODIS for two different time periods (1992–2000 and 2000–2017) yielded similar delineations of arid and semiarid areas, as shown in Fig. 3. As summarized in Table IV, arid regions are predominantly BSV, whereas semiarid regions were found to primarily consist of a mix of open shrubland, grassland, and BSV. The AVHRR-derived product was used for the development of SWAMPSv3 segment I (1992–1999), whereas the MODIS-based product was used for SWAMPSv3 segments II (2000–2008) and III (2009–2018). Differences in the arid/semiarid extent between these maps may arise from disparities in the NDVI products and/or the associated satellite sensors, as well as long-term changes in land cover. The latter was assumed to be the primary reason, but further improvements may benefit from quantifying the uncertainty in these modified classifications.

D. Evaluation of Surface Water Retrievals

SWAMPSv3 global f_w retrieval statistics and comparison with previous estimates are summarized in Fig. 4. The SWAMPSv3 monthly time series observe an overall reduction in total estimated inundated area in comparison to SWAMPSv2 because of the elimination of coastal waters. A static benchmark value of permanent inland water reported by the Landsat-derived G3WBM product [4], shown in the time series in Fig. 4, is ∼3.94 km ×105 km less (−13.2%) than the lowest annual minimum estimated by SWAMPSv3. This difference can potentially be attributed to greater f_w sensitivity and a richer time series unlimited by cloud cover provided by SWAMPS, in addition to inherent algorithm retrieval differences.

The mean annual statistics of SWAMPSv3 show a large concentration of f_w found in boreal regions (e.g., Canada, Scandinavia, and Western Siberia). This distribution pattern is consistent with findings from previous works [4]–[6]. For most of the globe, differences between SWAMPSv3 and SWAMPSv2 in mean annual statistics are within ±2%. Increases in both annual maximum and minimum f_w are observed primarily in boreal regions, largely because of the inclusion of permanent waters. Increases in annual f_w standard deviation are found primarily in areas affected by snow cover/melt because of changes in snow masking. Decreases in f_w are mostly seen across all shorelines and in the deserts of North Africa and the Arabian Peninsula. Although the inclusion of permanent waters slightly increased the f_w observed in known complex wetlands areas, underestimation of dynamic surface inundation under dense vegetation canopies remains a challenge related to the fundamental radiometric limitations that impact direct observations of surface conditions.

E. Data Availability

In accordance with NASA's free and open access data policy, SWAMPSv3 and full documentation supporting its assembly are available through the Alaska Satellite Facility, Fairbanks, AK, USA [25]. Segment I (1992–1999) is composited at a bimonthly time scale, whereas segments II (2000–2008) and III (2009–2018) are posted at a daily time step. As of this writing, the stable product extends from January 1, 1992, to December 31, 2018, and is updated monthly pending the release of ancillary data inputs. The NRT product is generated daily with a 2–3-day latency based on observed T_b and σ^0 along with the climatologies of hourly MERRA-2 atmospheric variables, 8-day MODIS snow cover, and 16-day MODIS NDVI each calculated over a 10-year period, 2008–2017.

IV. CONCLUSION

The newly released SWAMPSv3 has been developed to address limitations in the original SWAMPS data record under a NASA-sponsored uncertainty assessment effort. Reprocessing of the passive and active microwave data record produced a more consistent long-term time series and exclusion of nonterrestrial, coastal ocean and inland lake influences in reported f_w. Reliance on additional data inputs to further distinguish land cover classes may have contributed new sources of uncertainty but has successfully reduced anomalous retrievals in arid and semiarid regions. Continued work will focus on enhancing spatial resolution, overall accuracy, and sensitivity to subcanopy inundation. This more reliable and consistent long-term inundation record will benefit a number of applications including carbon modeling

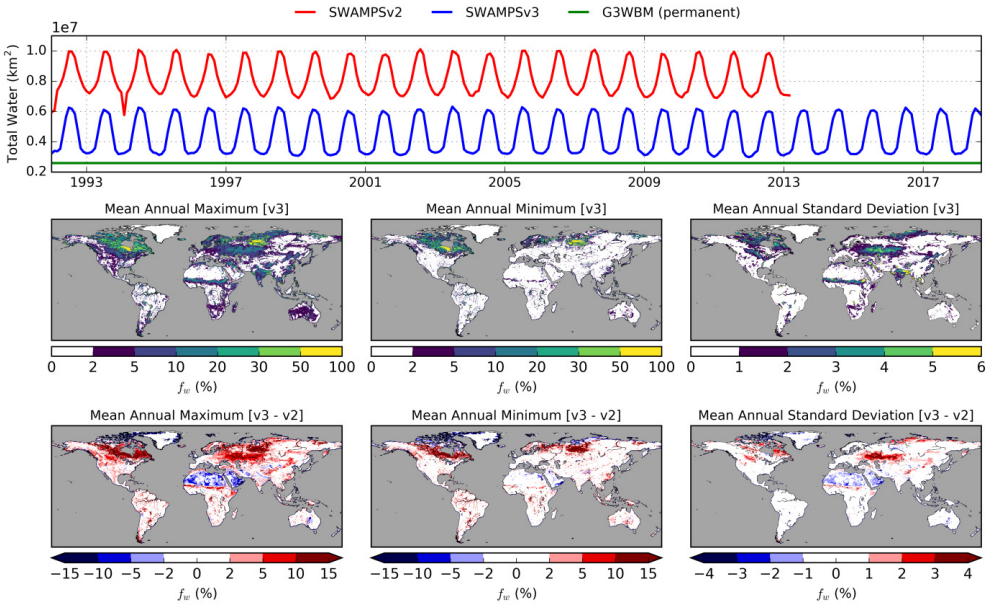

Fig. 4. Comparison of global SWAMPS f_W retrievals. (Top row) Monthly averaged time series of total global surface water area estimated by SWAMPSv2 (red) and the updated SWAMPv3 (blue). Static permanent inland water estimated by G3WBM [4] is shown in green. (Center row) Global SWAMPSv3 mean annual f_W (Left) maximum, (Center) minimum, and (Right) standard deviation. (Bottom row) Difference in global mean annual f_W (Left) maximum, (Center) minimum, and (Right) standard deviation observed between updated and previous SWAMPS [v3–v2]. Annual statistics is calculated from 1992 to 2012.

efforts, flood mapping, and general assessment of global responses to climate change.

REFERENCES

[1] S. Kirschke *et al.*, "Three decades of global methane sources and sinks," *Nat. Geosci.*, vol. 6, no. 10, pp. 813–823, Oct. 2013.

[2] M. Saunois *et al.*, "The global methane budget 2000–2012," *Earth Syst. Sci. Data*, vol. 8, no. 2, pp. 697–751, Dec. 2016.

[3] C. Lamarche *et al.*, "Compilation and validation of SAR and optical data products for a complete and global map of inland/ocean water tailored to the climate modeling community," *Remote Sens.*, vol. 9, no. 1, p. 36, Jan. 2017. doi: 10.3390/rs9010036.

[4] D. Yamazaki, M. A. Trigg, and D. Ikeshima, "Development of a global~90 m water body map using multi-temporal Landsat images," *Remote Sens. Environ.*, vol. 171, pp. 337–351, Dec. 2015.

[5] J.-F. Pekel, A. Cottam, N. Gorelick, and A. S. Belward, "High-resolution mapping of global surface water and its long-term changes," *Nature*, vol. 540, no. 7633, pp. 418–422, Dec. 2016.

[6] R. Schroeder *et al.*, "Development and evaluation of a multi-year fractional surface water data set derived from active/passive microwave remote sensing data," *Remote Sens.*, vol. 7, no. 12, pp. 16688–16732, Dec. 2015. doi: 10.3390/rs71215843.

[7] A. Sweeney *et al.* (May 2014). *Utilizing Remote Sensing to Explore Environmental Factors of Visceral Leishmaniasis in South Sudan*. IEEE Earthzine. Accessed: Sep. 26, 2018. [Online]. Available: https://earthzine.org/utilizing-remote-sensing-to-explore-environmental-factors-of-visceral-leishmaniasis-in-south-sudan/

[8] T. J. Bohn *et al.*, "WETCHIMP-WSL: Intercomparison of wetland methane emissions models over West Siberia," *Biogeosciences*, vol. 12, no. 11, pp. 3321–3349, Jun. 2015. doi: 10.5194/bg-12-3321-2015.

[9] B. Poulter *et al.*, "Global wetland contribution to 2000–2012 atmospheric methane growth rate dynamics," *Environ. Res. Lett.*, vol. 12, no. 9, Sep. 2017, Art. no. 094013. doi: 10.1088/1748-9326/aa8391.

[10] R. Gelaro *et al.*, "The modern-era retrospective analysis for research and applications, version 2 (MERRA-2)," *J. Climate*, vol. 30, no. 14, pp. 5419–5454, May 2017. doi: 10.1175/JCLI-D-16-0758.1.

[11] C. D. Kummerow, W. K. Berg, M. R. P. Sapiano, and N. C. Program. (2013). *NOAA Climate Data Record (CDR) of SSM/I and SSMIS Microwave Brightness Temperatures, CSU Version 1*. NOAA National Climatic Data Center. [Online]. Available: https://data.nodc.noaa.gov/cgi-bin/iso?id=gov.noaa.ncdc:C00827

[12] EUMETSAT. (Nov. 2008). *ERS Scatterometer Product version 1.6*. [Online]. Available: http://projects.knmi.nl/scatterometer/ers_prod/

[13] Q. Project, *SeaWinds on QuikSCAT Level 1B Time-Ordered Earth-Located Sigma0 Version 2*. California, CA, USA: PO.DAAC, Jul. 2006. doi: 10.5067/QSXXX-L1B02.

[14] EUMETSAT. *ASCAT Level 1B Product*. Accessed: Dec. 2013. [Online]. Available: https://www.avl.class.noaa.gov/saa/products/search?datatype_family=ASCAT

[15] *GIMMS AVHRR Global NDVI Version 1*. Global Inventory Monitoring and Modeling System (GIMMS) Project. Accessed: Jun. 18, 2017. [Online]. Available: https://ecocast.arc.nasa.gov/data/pub/gimms/

[16] K. Didan, *MOD13C1 MODIS/Terra Vegetation Indices 16-Day L3 Global 0.05Deg CMG V006*, NASA EOSDIS LP DAAC, Sioux Falls, SD, USA, 2015. doi: 10.5067/MODIS/MOD13C1.006.

[17] R. Armstrong, M. J. Brodzik, K. Knowles, and M. Savoie, *Global Monthly EASE-Grid Snow Water Equivalent Climatology, Version 1*. Boulder, CO, USA: NASA NSIDC, 2005. doi: 10.5067/KJVERY3MIBPS.

[18] D. K. Hall and G. A. Riggs, *MODIS/Terra Snow Cover 8-Day L3 Global 0.05Deg CMG, Version 6*. Boulder, CO, USA: NASA NSIDC, 2016. doi: 10.5067/MODIS/MOD10C2.006.

[19] R. Armstrong, K. Knowles, M. J. Brodzik, and M. A. Hardman, *DMSP SSM/I-SSMIS Pathfinder Daily EASE-Grid Brightness Temperatures, Version 2*. Boulder, CO, USA: NASA NSIDC, 1994. doi: 10.5067/3EX2U1DV3434.

[20] D. G. Long and P. J. Hardin, "Vegetation studies of the Amazon basin using enhanced resolution Seasat scatterometer data," *IEEE Trans. Geosci. Remote Sens.*, vol. 32, no. 2, pp. 449–460, Mar. 1994.

[21] K. Knowles, *EASE-Grid Land Cover Classifications Derived from Boston University MODIS/Terra Land Cover Data, Version 1*. Boulder, CO, USA: NASA NSIDC, 2004. doi: 10.5067/J0CJG7RZW3IJ.

[22] N. C. Grody and F. Weng, "Microwave emission and scattering from deserts: Theory compared with satellite measurements," *IEEE Trans. Geosci. Remote Sens.*, vol. 46, no. 2, pp. 361–375, Feb. 2008.

[23] W. R. Wieder, J. Boehnert, G. B. Bonan, and M. Langseth, *Regridded Harmonized World Soil Database v1.2. Data Set*. Oak Ridge, TN, USA: ORNL DAAC, 2014. doi: 10.3334/ORNLDAAC/1247.

[24] M. Gamo, M. Shinoda, and T. Maeda, "Classification of arid lands, including soil degradation and irrigated areas, based on vegetation and aridity indices," *Int. J. Remote Sens.*, vol. 34, no. 19, pp. 6701–6722, Oct. 2013. doi: 10.1080/01431161.2013.805281.

[25] K. Jensen and K. McDonald, *Surface Water Microwave Product Series, Version 3.2.*, ASF, Fairbanks, AK, USA, 2018. doi: 10.5067/SWAMPS3.2.